Analysis of Cable Overvoltages in Symmetrical Monopolar and Rigid Bipolar HVDC Configuration

Max Goertz, Simon Wenig, *Member*, *IEEE*, Simon Beckler, Carolin Hirsching, Michael Suriyah, *Member*, *IEEE*, and Thomas Leibfried, *Member*, *IEEE*

***Abstract*—The symmetrical monopolar configuration is the prevailing scheme configuration for high voltage direct current (HVDC) interconnectors utilizing the modular multilevel converter (MMC) topology. However, the rigid bipolar configuration is gaining significance, as first projects are currently in planning stage. The purpose of this paper is an analysis of both HVDC scheme configurations with regard to cable voltage stresses originating from short-circuit faults. The study focuses on HVDC cables with extruded insulation connected to MMCs equipped with half-bridge (HB) submodules. Basic design aspects in rigid bipolar configuration such as the station grounding concept are discussed. Moreover, various station internal as well as dc faults are examined by means of electromagnetic transient (EMT) simulations. Occurring cable voltage stresses are analyzed with respect to voltage polarity, peak value and wave front-parameters and compared in symmetrical monopolar and rigid bipolar configuration. It is demonstrated that cable overvoltages with same polarity as the dc operating voltage are significantly reduced in schemes operating in rigid bipolar configuration. Voltage reversals caused by the discharge process during a cable fault are nearly independent of the selected scheme configuration. Obtained results are relevant with regard to upcoming projects in rigid bipolar configuration and provide insights to further refine insulation co-ordination aspects related to dc cable systems.**

***Index Terms*—Bipolar configuration, extruded dc cable, half-bridge, insulation co-ordination, MMC-HVDC.**

I. Introduction

DURING the past decade, MMC technology gained a significant share of the HVDC market due to many technical and economic benefits such as required foot print of converter stations, operational flexibility and independent control of active and reactive power [1]. The introduction of MMC-HVDC boosted the installation of dc cables with extruded insulation, since MMC technology enables reversal of power flow direction without inversion of voltage polarity [2]. As the dc cable system is generally associated with large investment costs, a profound analysis of cable overvoltages by means of EMT-software is of significant importance to ensure a reliable insulation co-ordination strategy. The relevance of such preliminary EMT-studies increases due to the fact that present testing recommendations for dc cables with extruded insulation [3], [4] leave the specification of testing levels open for the customer-supplier negotiation process [5]. So far, the symmetrical monopolar (SMP) configuration represents the state-of-the-art for MMC-HVDC links [5]. But, triggered by a demand for higher power transfer capacities and consequently also dc voltage levels, the first MMC-HVDC projects in bipolar configuration are currently under construction [6]–[8]. Bipolar schemes without earth return or dedicated metallic return are called *rigid bipolar* (RBP) configuration [9]. From an economic viewpoint, the RBP configuration might provide benefits for long dc cable interconnectors as an avoidance of a third cable, namely the dedicated metallic return cable, reduces investment costs. In contrast to the SMP configuration, RBP schemes can operate at reduced transmission capacity in case of a converter failure or converter maintenance. However, - similar to SMP schemes - the RBP configuration does not provide redundancy in case of a cable failure.

As a consequence of the technical maturity of schemes in SMP configuration, many publications authored by the scientific community, system operators and manufacturers have analyzed the system behaviour during faults and subsequent converter blocking. The mechanism causing an overvoltage during dc side faults is explained in [10], while system studies related to insulation co-ordination aspects of dc cable systems and converter equipment are conducted in [11]–[14] and [15], respectively. However, existing literature with a focus on cable overvoltages in SMP configuration [10], [14] only analyzes the overvoltages at the cable terminations for selected fault types. For a comprehensive overvoltage analysis the spatial dependency of the overvoltage along the cable route has to be taken into account due to the fact that highest overvoltages occur inside the cable, as previously demonstrated in [12]. In addition, the worst case fault with regard to voltage reversals affecting the cable system is not covered in [10], [14]. The impact of project dependent parameters, like cable length on front time and peak value of the overvoltage, are outlined in [12], [16]. Moreover, [17] presents operational experience of a system operator and provides measured data during a cable fault. Recently published literature with regard to SMP schemes focuses on high voltage testing of dc cable systems and evaluates how representative overvoltage wave shapes might be generated [18], [19]. In contrast to the well-established SMP configuration, research focusing on system studies in RBP configuration is scarce due to limited project and operational experience [19], [20]. This paper is intended to fill this gap by providing a profound analysis and comparison of occurring cable voltage stresses in both system configurations. Compared to previously published literature [12], [20] the scope is fundamentally expanded. To completely

M. Goertz, C. Hirsching, M. Suriyah and T. Leibfried are with the Institute of Electric Energy Systems and High-Voltage Technology, Karlsruhe Institute of Technology, Karlsruhe, 76131, Germany (e-mail: max.goertz@kit.edu; carolin.hirsching@kit.edu; michael.suriyah@kit.edu; thomas.leibfried@kit.edu).

S. Wenig and S. Beckler are with TransnetBW GmbH, Stuttgart, 70191, Germany (e-mail: s.wenig@transnetbw.de; s.beckler@transnetbw.de).

This article has been accepted for publication in a future issue of this journal, but has not been fully edited. Content may change prior to final publication. Citation information: DOI 10.1109/TPWRD.2019.2960851, IEEE Transactions on Power Delivery

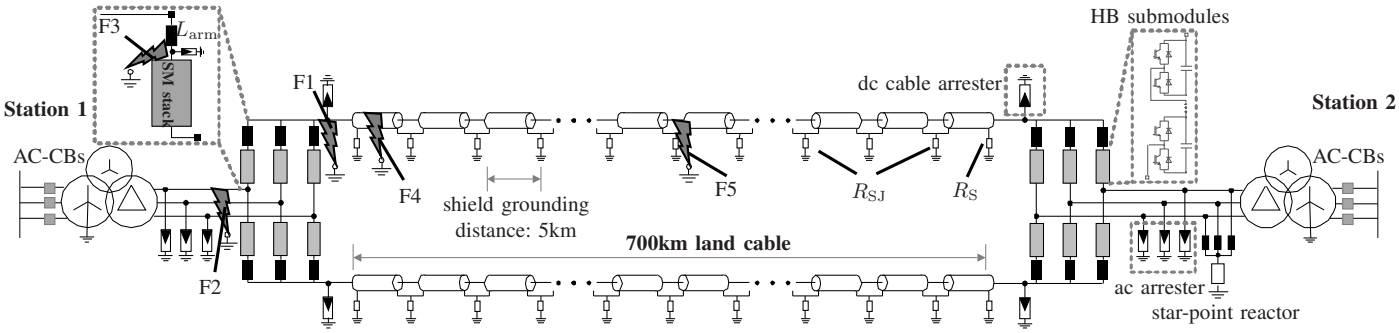

Fig. 1. Schematic of symmetrical monopolar configuration.

unveil the cable voltage stresses in both scheme configurations, various fault types are investigated by means of a parametric study approach and occurring cable voltage stresses are systematically evaluated with respect to voltage polarity, peak values and wave front-parameters. The findings of this paper provide a profound basis for further targeted discussions on HVDC cable systems subjected to non-standard voltage wave shapes and related overvoltage testing issues, as previously initiated in [16], [19], [21]. On top of existing literature, this paper highlights essential design aspects related to scheme configuration which gain in significance for schemes operating in RBP configuration, such as the station grounding concept and related impacts on the insulation co-ordination strategy of the cable. The scope of this research is especially relevant for upcoming HVDC projects dealing with long dc cable connections.

This paper is structured as follows. Section II describes the investigated schemes in SMP and RBP configuration, while the underlying modeling method applied in EMT-software is briefly outlined in Section III. Subsequently, Section IV focuses on station grounding design aspects in RBP configuration. A systematic approach to evaluate voltage stresses affecting the cable system as well as case study results are provided in Section V. Finally, a conclusion is given in Section VI.

II. System Description and Basic Design Aspects

In order to ensure a meaningful comparison between the SMP and RBP configuration, basic system parameter such as transmission capacity, rated dc voltage and submodule configuration are chosen identically in both schemes, as stated in Table I. The considered HVDC links are characterized by a total transmission capacity of 1GW and a rated dc voltage of $\pm 320\mathrm{kV}$. However, for the sake of completeness it should be mentioned that economic reasons behind the choice of the scheme configuration might lead to higher transmission power ratings and therefore possibly also to higher dc voltage ratings in the RBP configuration than in SMP schemes. The investigated scheme length of $700\mathrm{km}$ is motivated by the designated embedded HVDC links in Germany [22].

A. Symmetrical Monopolar MMC-HVDC

A simplified scheme of the considered SMP configuration is depicted in Fig. 1. Generally speaking, various project specific parameters such as station design, ac network characteristics and arrester co-ordination have influences on the system behaviour during contingencies, as shown in [15], [16]. Nevertheless, in order to achieve a generalized conclusion regarding the cable overvoltage characteristics, an illustrative SMP link configuration has been selected. Ac-circuit breakers (AC-CBs) are installed at the grid side of the converter transformer. The arm inductors are located on the dc side of the converters between submodule stacks and cable terminations. It should be noted that the arm inductors might also be installed on the converter ac side of each arm. However, in such systems an overvoltage characterized by a steep front and a high peak value might harm the dc cable in case of a converter internal fault between submodule stack and arm reactor, as explained in [15]. With regard to cable stresses, it is therefore recommended to either locate the arm inductors on the dc side or to install additional dc inductors. In the considered system, each arm of the MMC consists of 256 HB submodules with an average submodule voltage of $2.5\mathrm{kV}$.

TABLE I
Selected Parameters in SMP and RBP Configuration

Parameter	SMP	RBP
rated power per link P_{r}	1 GW	
rated dc voltage (pole-to-ground) U_0	$\pm$320 kV	
rated ac voltage (valve side)	330 kV	160 kV
rated ac voltage (grid side)	400 kV	
line frequency f	50 Hz	
short circuit level ac grid	45 GVA	
X/R ratio ac grid	10	
transformer configuration	wye-delta	
transformer leakage reactance	20 %	
number of submodules per valve arm	256	134
average arm sum voltage	640 kV	335 kV
average submodule voltage	2.5 kV	
submodule capacitor C_{S} (absolute)	8.5 mF	
submodule capacitor C_{S} (relative)	39 kJ/MVA	41 kJ/MVA
arm inductance L_{arm}	50 mH	
clearing time ac circuit breakers T_{C}	80 ms	
grounding resistor R_{G}	–	see Sec. IV

This article has been accepted for publication in a future issue of this journal, but has not been fully edited. Content may change prior to final publication. Citation information: DOI 10.1109/TPWRD.2019.2960851, IEEE Transactions on Power Delivery

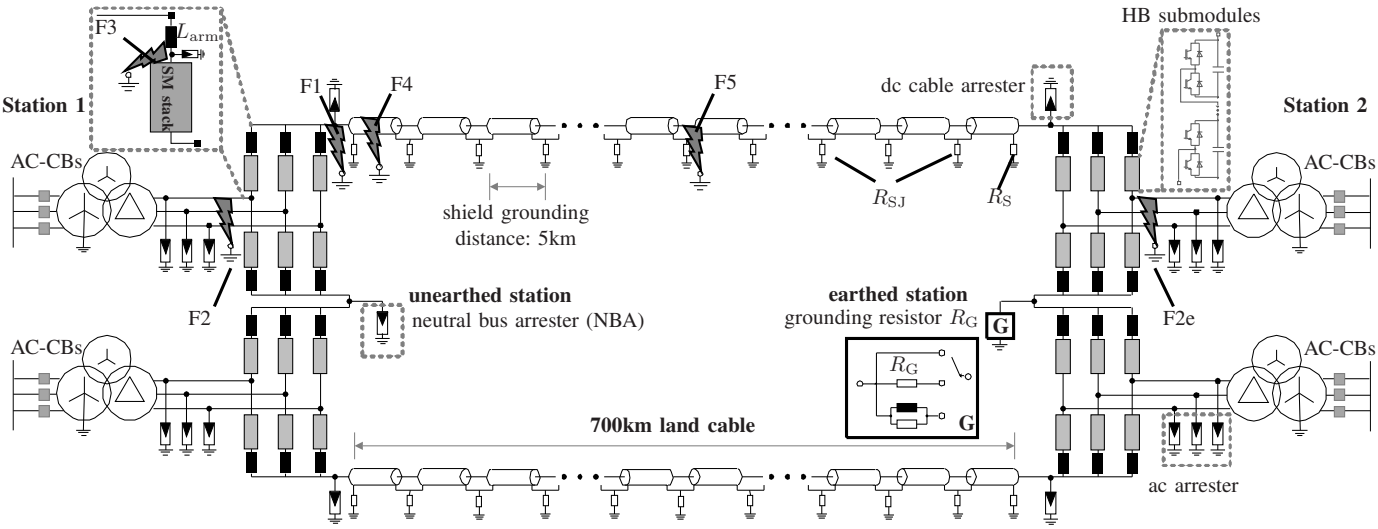

Fig. 2. Schematic of rigid bipolar configuration.

As a consequence of the 3rd harmonic injection applied in HB-MMC HVDC systems to optimize the required number of submodules, a high zero-sequence impedance is required on transformer valve side under normal operation [23]. Here, the most commonly used wye-delta transformer vector group is considered. The star-point reactor at station 2 ensures a symmetrization of the dc voltages at both dc poles relative to ground potential [24]. During transient events the contribution of the star-point reactor to the fault current is marginal, which is due to the high impedance of the star-point reactor. For the sake of completeness, it should be mentioned that the transformer vector group as well as the applied grounding configuration on converter valve side are dependent on project specific requirements and the selected converter manufacturer. Other design variants comprise a wye-wye transformer in combination with a surge arrester connected to the star point of the wye winding at transformer valve side [25]. The impact of transformer vector group and grounding on temporary overvoltages (TOV) originating from dc side faults is outlined in [17], [25]. In assessing representative overvoltages affecting the cable system, a typical arrester arrangement is considered to protect converter equipment and cable system [26]. The residual voltages of the arrester groups during a current impulse with a 30/60µs wave shape are stated in Table II.

B. Rigid Bipolar MMC-HVDC

In contrast to the high-impedance grounding concept applied in SMP schemes, bipolar systems are low-impedance grounded at the neutral point on the dc side of at least one converter station [9]. In case permanent earth return currents are prohibited, the neutral point is earthed at a single station and protected by an arrester bank at the other station. Such a system, called RBP, is depicted in Fig. 2. Corresponding parameters of the considered RBP scheme are stated in Tab. I. A generalized overview of possible grounding options for monopolar and bipolar systems and their impact on fault behaviour is conducted in [27]. As indicated in Fig. 2, several grounding options are conceivable in RBP configuration: *i)* solid grounding, *ii)* grounding through an additional resistor R_G and *iii)* grounding through a parallel *R-L* circuit. The key design parameters in RBP configuration affecting overvoltage levels and fault current stresses are the grounding configuration and the protection level of the neutral bus arrester (NBA) located at the unearthed station [20]. This basic design aspect is discussed in Section IV. The switching impulse protective levels (SIPL) of the surge arresters used for the parametric study are stated in Tab. II.

III. Modeling Method

Generally, the depth of modeling for overvoltage studies in EMT-software represents a trade-off between computational burden and required accuracy of results. Moreover, the models of relevant system components have to be coherent with the frequency range related to the type of study. The overvoltage phenomena investigated within this study are in the range of temporary and slow-front overvoltages according to the classification given in [28].

A. Converter Station

The submodule stacks are modeled using a detailed equivalent circuit model. This approach, classified in [29] as *Type 4* model, applies a circuit reduction in each time-step in order to reduce the number of electrical nodes in each MMC arm.

TABLE II
Arrester Parameters in SMP and RBP Configuration

Type of arrester	Switching impulse protective level (SIPL)	
	SMP	**RBP**
cable arrester	544 kV @ 3 kA	
ac arrester	493 kV @ 3 kA	510 kV @ 3 kA
neutral bus arrester	–	150 kV @ 10 kA

This article has been accepted for publication in a future issue of this journal, but has not been fully edited. Content may change prior to final publication. Citation information: DOI 10.1109/TPWRD.2019.2960851, IEEE Transactions on Power Delivery

Moreover, a Thevenin equivalent is used to represent the ac grid and corresponding short circuit level. The switching impulse characteristics of the surge arresters are represented through piece-wise linear resistors. A series inductance representing the lead wire of the arrester is taken into account.

B. Converter Control and Protection

Prior to fault occurrence, station 1 operates in active/reactive power control mode and station 2 is in dc voltage/reactive power control mode in both considered scheme configurations. A general overview of the considered control architecture is reported in [29]. Further details concerning the quasi-decoupled control approach of ac, dc as well as converter internal quantities are provided in [30]. In general, MMC-HVDC stations are equipped with hierarchical protection systems that allow an appropriate protection co-ordination philosophy according to the grid code requirements and project dependent specifications [1], [31]. Within this study, a simplified protection algorithm is used, in which the detection of a fault leads to a permanent block of the converter followed by a trip of AC-CBs. Due to the lack of redundancy in the event of a cable fault in RBP configuration, both converters of a station block their IGBTs when a cable fault or a station internal fault is detected. In both considered scheme configurations, each station is equipped with an independent protection system that comprises several functions: *i)* valve overcurrent protection, *ii)* submodule under-/overvoltage protection, *iv)* dc under-/overvoltage protection and *iv)* dc pole-to-ground voltage unbalance protection. The protection loops include artificial delays to account for imperfection due to data acquisition and processing, as indicated in Fig. 14 found in the Appendix.

C. Cable System and Accessories

A cable system with extruded insulation feasible for land installation is considered. The cable consists of a copper conductor with a cross-section of $2500\mathrm{mm}^2$, inner semiconductive layer, main insulation, outer semi conductive layer, metallic screen and outer sheath. Both dc cables are laid in flat formation in a depth of $1.3\mathrm{m}$ below ground surface. The frequency-dependent cable model available in PSCAD/EMTDC based on the theory given in [32] is used. The cable shields are bonded at connection joints and solidly grounded every $5\mathrm{km}$. The bonding lead connecting the cable sheath to local ground is modeled with lumped *R-L* elements. Grounding resistances of $R_{\mathrm{SJ}} = 5\Omega$ and $R_{\mathrm{S}} = 0.1\Omega$ are taken into account at joints and cable terminations, respectively. The inductance of the bonding lead is $L = 5\mu\mathrm{H}$, following the assumption of $1\mu\mathrm{H/m}$ given in [28].

IV. Rigid Bipole: Impact of Station Grounding

Prior to a systematic overvoltage analysis, it is necessary to outline relevant basic station design aspects in the RBP configuration. Therefore, this section is intended to point out the impact of the station grounding concept on fault current stresses and cable overvoltages and to mention related design considerations.

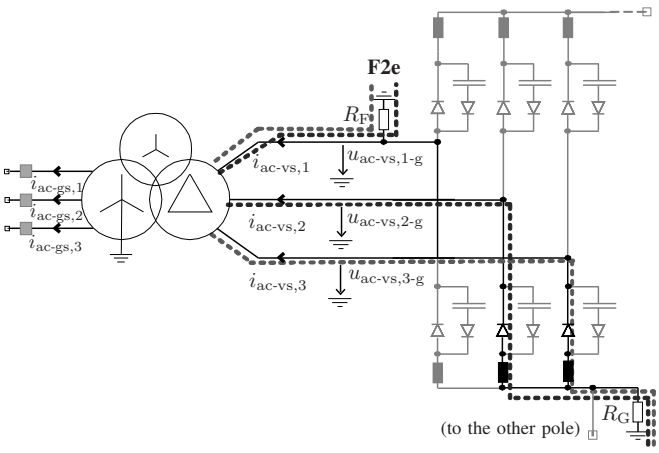

Fig. 3. Simplified equivalent circuit after IGBT blocking during a single phase-to-ground fault at transformer valve side (F2e) in RBP configuration.

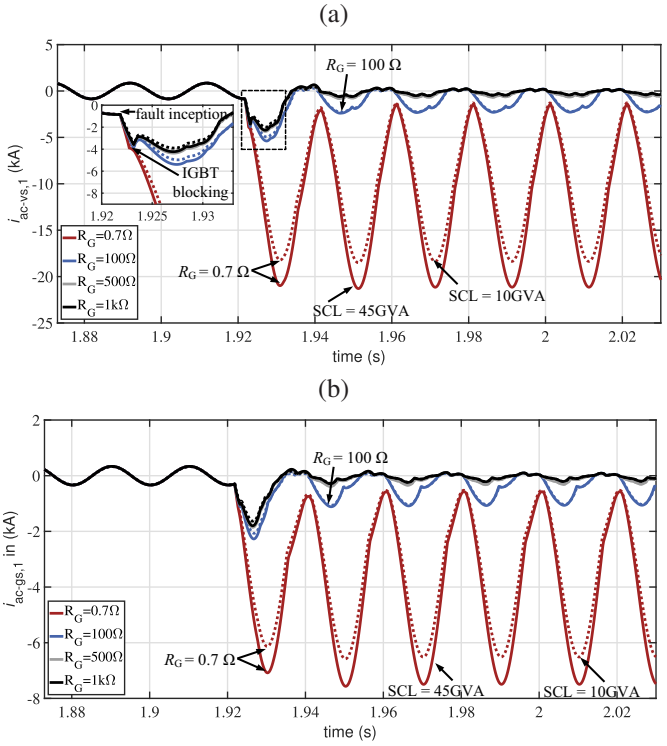

Fig. 4. Impact of station grounding resistance R_{G} on fault current stresses during a single phase to ground fault at transformer valve side (F2e) in RBP configuration: (a) current in phase 1 at transformer valve side, (b) current in phase 1 on transformer grid side.

A. AC Fault on Transformer Valve Side

For HB-MMC schemes operating in bipolar or asymmetric monopolar configuration, special consideration has to be given to single phase-to-ground faults at the transformer valve side. Such a fault might occur in case of a failure of a transformer- or valve hall bushing. The relevance of this fault type with regard to basic design aspects is outlined for a phase 1-to-ground fault at the earthed station (F2e), see Fig. 2. For a comprehensive system analysis of the converter internal voltage and current stresses during F2e the reader is referred

This article has been accepted for publication in a future issue of this journal, but has not been fully edited. Content may change prior to final publication. Citation information: DOI 10.1109/TPWRD.2019.2960851, IEEE Transactions on Power Delivery

to [33]. However, in contrast to [33] where the focus is laid on bipolar systems with earth return with a view mainly on converter stresses during F2e, this paper is intended to highlight the impact of the station grounding concept on the insulation co-ordination strategy of the cable system. When the fault F2e is detected, both converters of station 2 are blocked and a trip signal is sent to the AC-CBs. A simplified equivalent circuit of the upper converter of station 2 after IGBT blocking is depicted in Fig. 3. During F2e, the phase-to-ground voltage of the faulty phase $u_{\text{ac-vs,1-g}}$ sags to zero, the voltages of the healthy phases $u_{\text{ac-vs,2-g}}$, $u_{\text{ac-vs,3-g}}$ rise to $\sqrt{3}$ times the ac component of the phase-to-ground voltage under normal operation, and the phase shift between the healthy phases is reduced to 60°. As a consequence, the anti-parallel diodes installed in the negative arms of healthy phases conduct and lead to fault current paths through the fault impedance R_{F}, converter transformer and the grounding electrode R_{G}. The fault currents in the faulty ac phase at transformer valve side (vs) $i_{\text{ac-vs,1}}$ and grid side (gs) $i_{\text{ac-gs,1}}$ during F2e are depicted in Fig. 4 for different station grounding options. Considered grounding options are solid grounding ($R_{\text{G}} = 0.7\Omega$) as well as grounding through an additional resistor R_{G} in the range of 100Ω up to $1\text{k}\Omega$. Results are shown for two different short circuit levels (SCL) characterizing a strong (solid lines) and a medium ac network strength (dashed lines). As clearly depicted, dc components are superimposed on ac currents at transformer grid and valve side. In case of solid station grounding ($R_{\text{G}} = 0.7\Omega$), the dc component leads to an absence of ac current zero crossings at transformer grid side. Due to the absence of current zero-crossings the AC-CBs might not be able to clear the fault. One possible countermeasure to mitigate the dc components is a resistive station grounding concept instead of a solid grounding [20]. The dc components as well as the fault current stresses of converter equipment and transformer decrease with increasing values of R_{G}, see Fig. 4. However, also for solidly grounded schemes other countermeasures exist to ensure current zero-crossings during F2e. The measure mentioned in [34], [35] proposes the installation of auxiliary earthing breakers with grounding resistors at transformer grid side. As indicated in [35], the auxiliary breakers are closed during F2e and create a three-phase short circuit through the grounding resistors on transformer grid side. This measure ensures current zero-crossings and enables the AC-CBs to clear the fault. However, the impact of the artificial short circuit on the ac grid is not discussed in [35].

B. DC Cable Fault

In order to highlight the relevance of the grounding concept with regard to the insulation co-ordination strategy of the cable system, system behaviour is outlined for a dc side fault. The cable fault occurs along the positive dc pole at 50% of the scheme length (F5). As discussed in [20], the cable connected to the negative pole is subjected to an overvoltage during F5. The voltage at the healthy dc pole is shown in Fig. 5 for the considered grounding options. The overvoltage level affecting the cable system rises with increasing values of R_{G}. To illustrate the effect of the NBA at the unearthed station on

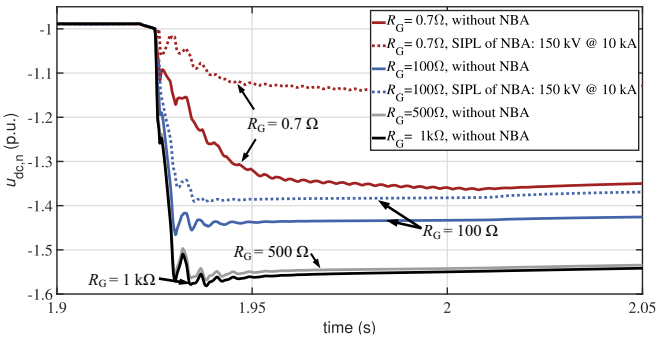

Fig. 5. Impact of station grounding resistance R_{G} and neutral bus arrester (NBA) on cable overvoltage, depicted in per unit of rated dc voltage during dc fault F5 in RBP configuration.

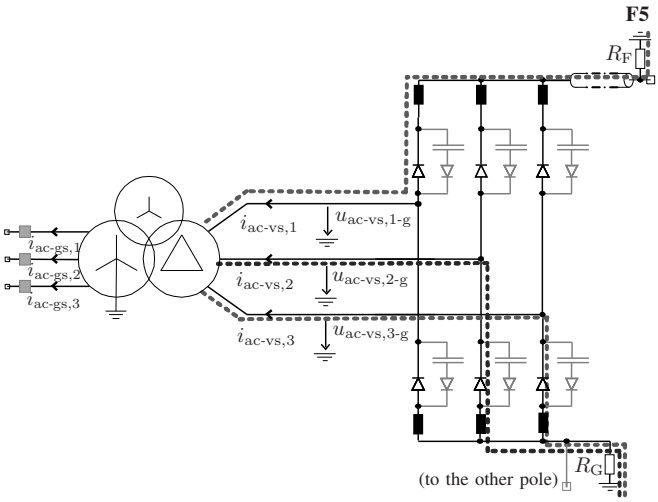

Fig. 6. Simplified equivalent circuit after IGBT blocking in the event of a dc fault in RBP configuration for one possible diode conduction state.

system behaviour, the overvoltage with NBA (dashed lines) and without NBA (solid lines) in service is highlighted in Fig. 5. A simplified equivalent circuit of the upper converter at the earthed station after IGBT blocking is depicted in Fig. 6. The anti-parallel diodes lead to fault current paths through the fault impedance R_{F}, the cable system, converter transformer and the grounding electrode R_{G}, or instead the NBA at the unearthed station, as long as AC-CBs have not cleared the fault. With regard to the required insulation level of the dc cable system, solid neutral bus earthing is beneficial in order to reduce the cable overvoltage during dc side faults. On the contrary, solid neutral bus earthing might lead to high fault current stresses of power electronic devices and to an absence of ac current zero-crossings in the event of a station internal ac fault. Therefore, grounding philosophy in RBP configuration represents a key design compromise between permissible fault current stresses and overvoltage limitations. The following parametric study focuses on two different station grounding options: *i)* solid grounding ($R_{\text{G}} = 0.7\Omega$) as well as *ii)* additional grounding resistor of $R_{\text{G}} = 100\Omega$. Both grounding concepts are considered as feasible layout options for schemes in the RBP configuration.

This article has been accepted for publication in a future issue of this journal, but has not been fully edited. Content may change prior to final publication. Citation information: DOI 10.1109/TPWRD.2019.2960851, IEEE Transactions on Power Delivery

V. Cable Overvoltage Characteristics

A. Parametric Study Approach

The following sections focus on the assessment of representative cable overvoltages in SMP and RBP configuration. In light of the variety of parameters affecting the fault behaviour, several pre-fault converter operation modes and various station internal as well as cable faults are taken into account, as summarized in Tab. III. Similar parametric study approaches are performed in [12], [15], [16]. In order to determine the most critical fault instant with regard to the cable overvoltage, the fault occurrence is varied at different time instants over one cycle of ac current or phase-to-ground voltage at transformer valve side of station 1. In order to cover the spatial dependency of the cable overvoltage, multiple voltage measurement points are located every 5% of scheme length. As a first step, several parametric studies are performed by means of EMT-software. Then, obtained data are post-processed and cable voltages measured along the positive dc pole $u_{\mathrm{dc,p}}$ and the negative dc pole $u_{\mathrm{dc,n}}$ are analyzed at each voltage measuring point with respect to: *i)* voltage polarity, *ii)* peak value, *iii)* time-to-peak value and *iv)* voltage gradient.

B. Overvoltage Levels

Depending on the fault location, the dc cable might be subjected to an overvoltage with same polarity as the dc operating voltage U_0 or to a voltage reversal. The highest peak values of all measured voltages along the cables of both dc poles are depicted in Fig. 7. A peak value is here defined as the highest occurring crest value of either an overvoltage with same polarity as U_0 or of a voltage reversal. Results are shown for each fault type, scheme configuration and pre-fault converter operation mode. It is important to clarify that Fig. 7 contains the parametric study outcome of in total 1.500 EMT-simulations according to Tab. III. As a consequence of the investigated fault locations, an overvoltage with same polarity as U_0 can be observed at the cable of the negative dc pole in both scheme configurations. In SMP configuration, the highest peak value of overvoltages with same polarity as U_0 is 1.72 p.u. and occurs during a cable fault at 50% of scheme length (F5) at zero/low load operation. In RBP configuration, the highest peak value of overvoltages with same polarity as U_0 is significantly reduced compared to SMP schemes and is 1.33 p.u. ($R_{\mathrm{G}} = 0.7\Omega$, F5) or 1.55 p.u. ($R_{\mathrm{G}} = 100\Omega$, F3) depending on the applied station grounding concept. Voltage reversals might occur during the cable discharge process of the faulty dc pole, see Fig. 7 (b) for F1, F3-F5. The worst case voltage reversal of 0.96 p.u. can be observed during a cable fault in the vicinity of the converter station (F4) and is nearly independent of the scheme configuration and the applied grounding concept.

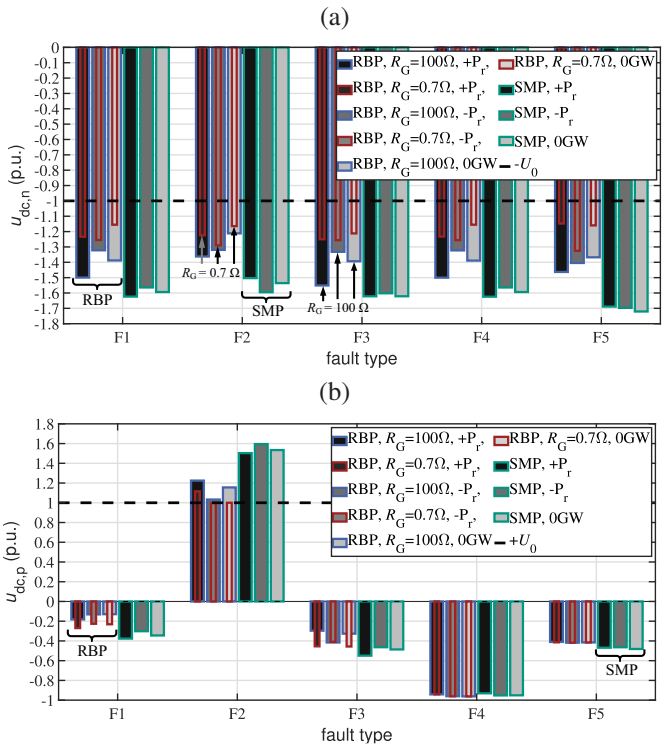

Fig. 7. Highest peak values of all measured voltages along the cable system for each fault type F1 - F5, power set point and scheme configuration: (a) measured voltages along negative dc pole, (b) measured voltages along positive dc pole.

TABLE III
Parametric Study Setup

	Description	Configuration
1.	power set point at station 1	a) $+P_{\mathrm{r}}$ (ac in-feed), $+Q_{\mathrm{r}}$ (cap.) b) $-P_{\mathrm{r}}$ (ac export), $+Q_{\mathrm{r}}$ (cap.) c) 0GW (zero load), $+Q_{\mathrm{r}}$ (cap.)
2.	fault type	F1: positive dc pole-to-ground fault at cable termination F2: phase 1-to-ground fault at transformer valve side F3: positive arm p1-to-ground fault F4: cable core-to-screen-to-ground fault at 1km distance from station 1 (positive pole) F5: cable core-to-screen-to-ground fault at 50% of scheme length (positive pole)
3.	fault resistance R_{F}	0.1Ω, 10Ω
4.	fault synchronisation	a) zero crossing of phase 1-to-ground voltage at transformer valve side b) zero crossing of ac current in phase 1 at transformer valve side
5.	fault instant	a) $\omega \cdot t = 0°$, b) $\omega \cdot t = 45°$ c) $\omega \cdot t = 90°$, d) $\omega \cdot t = 225°$ e) $\omega \cdot t = 270°$ after zero crossing

C. Spatial Dependency

Figure 8 shows the spatial dependency of the cable overvoltages along the route in SMP (dashed lines) as well as in RBP configuration (solid lines: $R_{\mathrm{G}} = 0.7\Omega$, dotted lines: $R_{\mathrm{G}} = 100\Omega$). The voltage profiles consist of the highest voltage peak values at each measuring point derived for all parameter variations related to the same fault type. In SMP configuration, the worst case overvoltage with same polarity as U_0 occurs in the middle of the cable of the healthy dc pole in case of F5. The overvoltage build-up during F5 can

This article has been accepted for publication in a future issue of this journal, but has not been fully edited. Content may change prior to final publication. Citation information: DOI 10.1109/TPWRD.2019.2960851, IEEE Transactions on Power Delivery

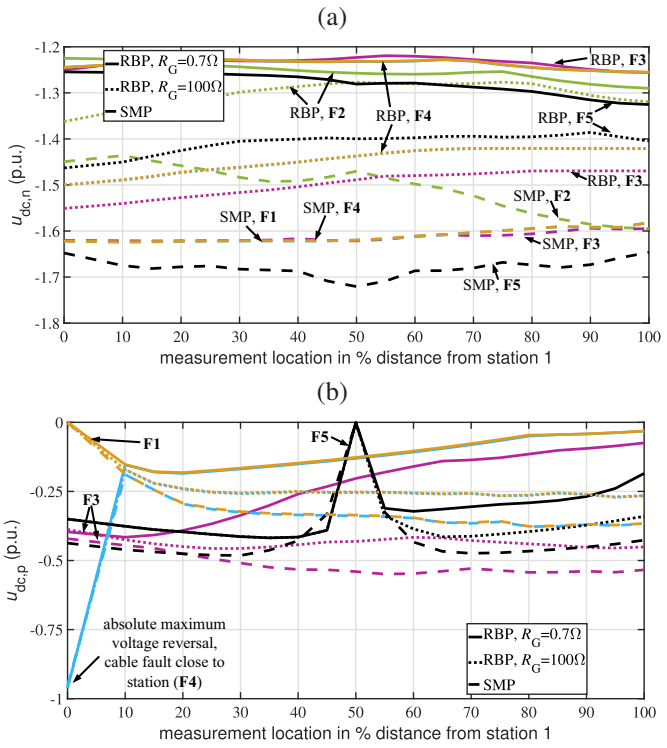

Fig. 8. Worst case voltage profiles along the cable system as a function of fault type F1 - F5 and scheme configuration: (a) negative dc pole, (b) positive dc pole.

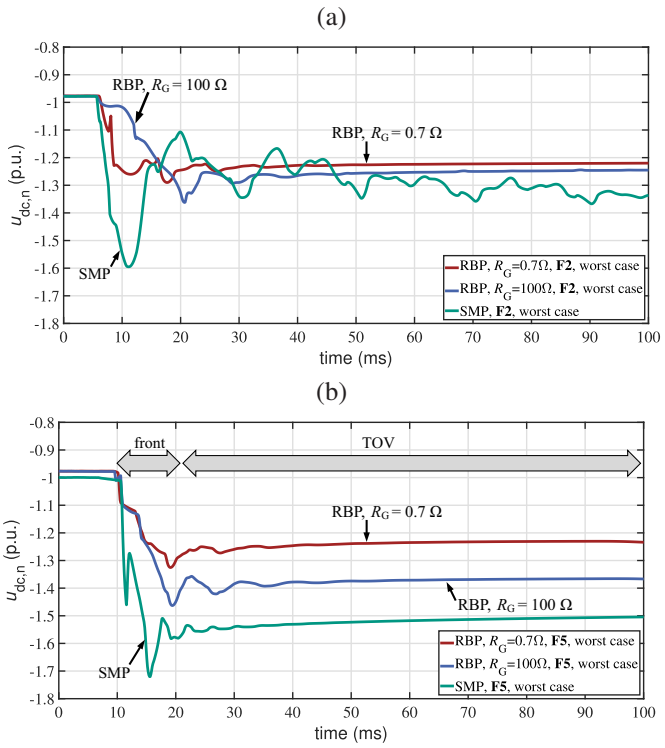

Fig. 9. Worst case cable overvoltage with same polarity as the dc operating voltage: (a) single phase-to-ground fault at transformer valve side (F2), (b) cable fault at 50% of scheme length (F5).

be explained by traveling wave phenomena, as shown in [12], [13]. In RBP configuration, the worst case cable overvoltage with same polarity as U_0 occurs either at the unearthed converter station or at the earthed station depending on the applied grounding concept. In all scheme configurations, the absolute maximum voltage reversal occurs at the cable termination adjacent to the faulty cable section, see Fig. 8 (b) for F4.

D. Worst Case Overvoltage Wave Shapes

A comparison between the worst case cable overvoltages with same polarity as U_0 occurring in SMP and RBP configurations is visualized in Fig. 9 (a)-(b). In both scheme configurations, the generalized overvoltage shape consists of an overvoltage front during which the peak value is reached, followed by a TOV at a decreased voltage level, as indicated in Fig. 9 (b). The level of the TOV depends on the opening instants of the AC-CBs, rated ac voltage on transformer valve side, the RBP station grounding concept and, in SMP configuration, on the discharge characteristic of the cable arresters. In both scheme configurations, the TOV persists until the cable is discharged through intrinsic shunt or stray impedances to ground or auxiliary earthing devices are applied, as discussed in [11], [20]. The absolute maximum voltage reversals are depicted in Fig. 10 for both scheme configurations. As can be seen, the system configuration has only limited impact on occurring voltage reversals. Instead, the voltage reversal is mainly caused by the intrinsic discharge process of the faulty cable section through the fault impedance and remains below 1 p.u., as explained in [11].

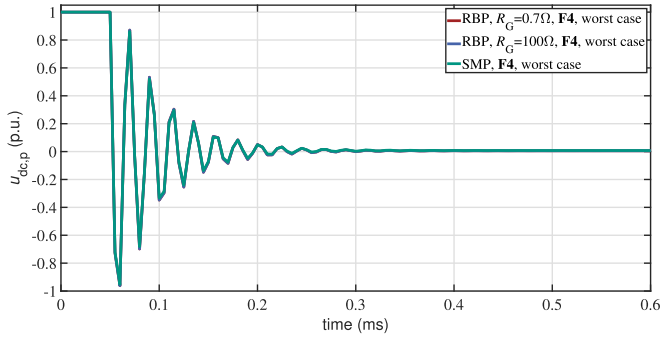

Fig. 10. Worst case cable voltage reversal occurring at the faulty cable during fault F4.

E. Overvoltage Front-Parameters

With regard to overvoltages with same polarity as U_0, further parameters characterizing the overvoltage front are evaluated. The time-to-peak value is here defined as the time interval between $\pm 5\%$ of U_0 and the point in time of the voltage peak value. Time-to-peak values are calculated at each measuring point along the cable taking into account all parameter sensitivities. Moreover, absolute maximum voltage gradients during the front of the overvoltage are determined. Then, fastest time-to-peak values and steepest voltage gradients of all measuring points along the cable under consideration of all parameter variations are ascertained, see Fig. 11. Fastest time-to-peak values are in the range of milliseconds for the scheme operating in SMP configuration and in the range of several hundreds of microseconds in RBP configuration. Moreover,

This article has been accepted for publication in a future issue of this journal, but has not been fully edited. Content may change prior to final publication. Citation information: DOI 10.1109/TPWRD.2019.2960851, IEEE Transactions on Power Delivery

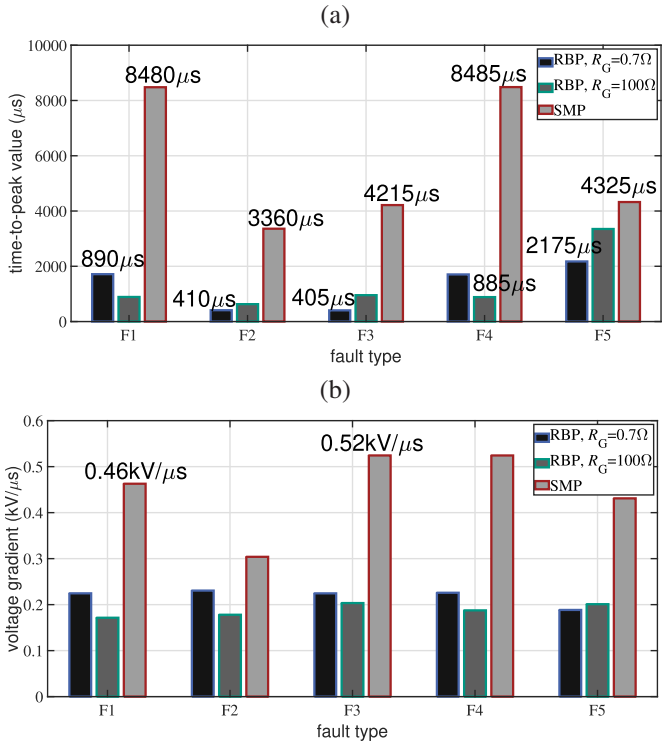

Fig. 11. Front-parameters of all cable overvoltages with same polarity as the dc operating voltage, depicted as a function of fault type and scheme configuration: (a) Fastest time-to-peak values, (b) absolute maximum voltage gradients.

steeper voltage gradients can be observed in the SMP configuration. However, it is worthwhile to mention that fastest time-to-peak values and highest overvoltage peak values occur not at the same measuring point and not for the same parameter combination. Especially in the RBP configuration, the parameter combinations that lead to the wave shape with the fastest front-times do not cause the highest overvoltage peak values. A combination of worst case values for testing purposes might therefore lead to unrealistic stresses. In addition, for the sake of completeness, it should be mentioned that time-to-peak values are strongly dependent on scheme length, as shown in [12] and further discussed in Section V-F.

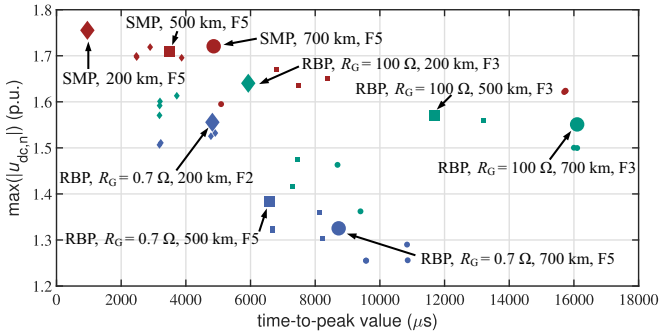

Fig. 12. Impact of cable length and scheme configuration on the absolute values of highest voltage peak values of all cable overvoltages with same polarity as the dc operating voltage and time-to-peak values of the associated wave shapes.

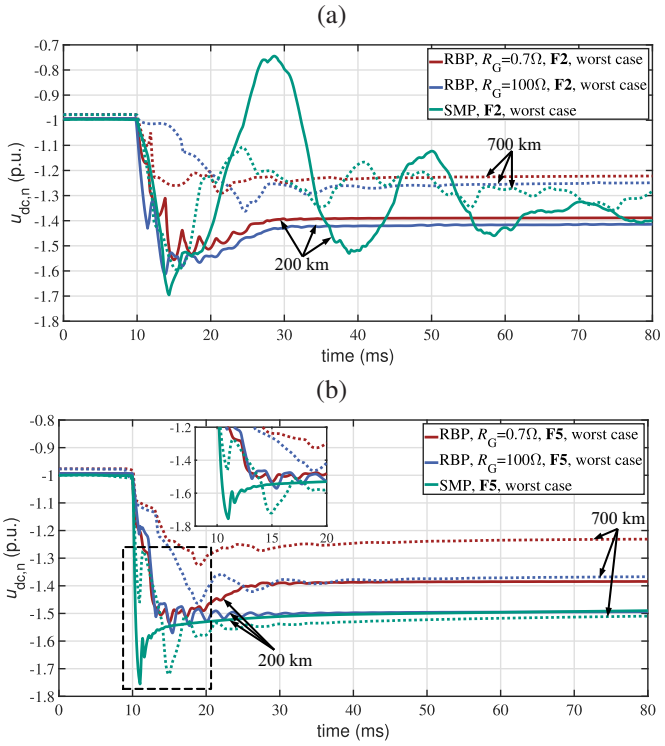

Fig. 13. Worst case cable overvoltage with same polarity as the dc operating voltage for different cable lengths: (a) single phase-to-ground fault at transformer valve side (F2), (b) cable fault at 50% of scheme length (F5).

F. Impact of Cable Length

In order to derive a more general statement concerning cable overvoltages, the impact of scheme length is investigated within this section. Therefore, the parametric studies as stated in Table III are repeated for cable lengths of 200 km and 500 km. The absolute values of the highest peak values of all cable overvolages with same polarity as U_0 are depicted in Fig. 12 for the investigated scheme configurations and cable lengths. In addition to each overvoltage level, the time-to-peak values of the associated voltage wave shapes are given. It is important to clarify that there exist faster time-to-peak values but these values occur for smaller overvoltage peak values. It should be mentioned that Fig. 12 contains the outcome of several thousands of EMT simulations. The large data points represent the worst case fault type of each scheme configuration and cable length with respect to the overvoltage peak values. The small data points indicate the worst case combination of the other fault types. As can be seen, the scheme length has a significant impact on the time-to-peak. Moreover, it is noticeable that highest overvoltage peak values occur for a cable length of 200 km in SMP as well as in RBP configuration. The differences in the overvoltage peak values between the RBP and the SMP configuration decrease with shorter cable lengths. In SMP configuration, the cable fault F5 causes the highest overvoltage peak values for all investigated cable lengths. In RBP configuration, highest voltage peak values can be observed during F3 or F2 and F5 depending on the applied station grounding concept and cable length. A comparison of the voltage wave shapes with the

TABLE IV
SCHEME DEPENDENT CHARACTERISTICS OF OVERVOLTAGES WITH SAME POLARITY AS U_0

	time-to-peak value of the wave shape leading to $\max(\lvert u_{\mathrm{dc,n}}\rvert)$			**absolute value of the highest overvoltage peak value** $\max(\lvert u_{\mathrm{dc,n}}\rvert)$			**absolute value of the highest TOV level**		
scheme length	200 km	500 km	700 km	200 km	500 km	700 km	200 km	500 km	700 km
RBP $R_{\mathrm{G}} = 0.7\Omega$	4820 µs	6590 µs	8725 µs	1.55 p.u.	1.38 p.u	1.33 p.u	1.43 p.u	1.31 p.u	1.27 p.u
RBP $R_{\mathrm{G}} = 100\Omega$	5930 µs	11700 µs	16100 µs	1.63 p.u.	1.56 p.u	1.55 p.u	1.50 p.u	1.50 p.u	1.48 p.u
SMP	955 µs	3500 µs	4860 µs	1.76 p.u	1.71 p.u	1.72 p.u	1.51 p.u	1.50 p.u	1.51 p.u

highest peak values occurring during F2 and F5 are depicted in Fig. 13 (a)-(b). For the sake of clarity, only cable lengths of 200 km and 700 km are shown. It is obvious that the initial voltage gradient during the overvoltage front increases for shorter cable lengths. Moreover, as can be seen in Fig. 13 (b) for the RBP scheme with 200 km cable length, the overvoltage front consists of a superposition of multiple traveling waves. In the 700 km system, the cable self attenuation effect mitigates the traveling waves propagating along the cable and leads to a reduced peak value. The mechanism of the overvoltage build-up during F5 in SMP configuration is explained in [12].

With regard to the impact of the cable length on the voltage reversals, it can be concluded that the highest peak value of the voltage reversals occurring at the cable system is not affected by the scheme length. As already mentioned in Section V-B, the worst case voltage reversal occurs during a cable fault in the vicinity of the converter station (F4) and is nearly independent of scheme configuration and total cable length.

G. Generalized Overvoltage Parameters

Table IV summarizes the relevant parameters of cable overvoltages with same polarity as U_0 occurring in the considered scheme configurations. Generally speaking, the RBP configuration provides considerable benefits with regard to the required overvoltage withstand capability of the cable system as occurring overvoltage peak values as well as TOV levels are significantly reduced compared to SMP schemes. However, these benefits of the RBP configuration are most pronounced for long scheme lengths. Moreover, it is important to keep in mind that especially in the RBP configuration manufacturer dependent station design aspects such as the station grounding concept affect the fault behaviour and thus overvoltage characteristics. For the sake of completeness, it should be pointed out that special consideration has to laid on cable overvoltages in case of HVDC schemes comprising mixed overhead-line and cable sections. Traveling wave phenomena might lead to more severe overvoltages in such systems, as indicated in [12].

VI. CONCLUSION

This paper facilitates a profound analysis and comparison of voltage stresses affecting the HVDC cable system in the SMP and the RBP configuration. Compared to state-of-the art SMP schemes, cable overvoltages occurring in RBP configuration are significantly smaller. From an insulation co-ordination point of view, this aspect might result in reduced requirements of the cable withstand voltage as well as in an increased equipment reliability. These issues might become a relevant benefit in projects comprising long cable routes as the cable system is then usually associated with a considerable share of total project costs. However, it should be kept in mind that the RBP configuration and in particular the applied station grounding concept represents a technical design compromise between fault current stresses and overvoltages. Especially in case of solid station grounding, auxiliary protection equipment is required in order to ensure zero-crossings of the ac fault currents in the event of station internal ac faults at transformer valve side. These findings regarding the impact of station design aspects on the insulation co-ordination strategy of the cable system represent a relevant contribution to the coordination processes between the prospective HVDC link owner, the cable supplier and the converter manufacturer. Moreover, the obtained overvoltage characteristics provide a basis for the currently ongoing discussion on HVDC cable systems subjected to non-standard voltage wave shapes and related overvoltage testing issues. Based on the determined overvoltage characteristics, future research is required in order to evaluate the impact of the non-standardized overvoltage shape on the cable insulation as well as on the aging process of the cable system.

APPENDIX

A. Protection Scheme

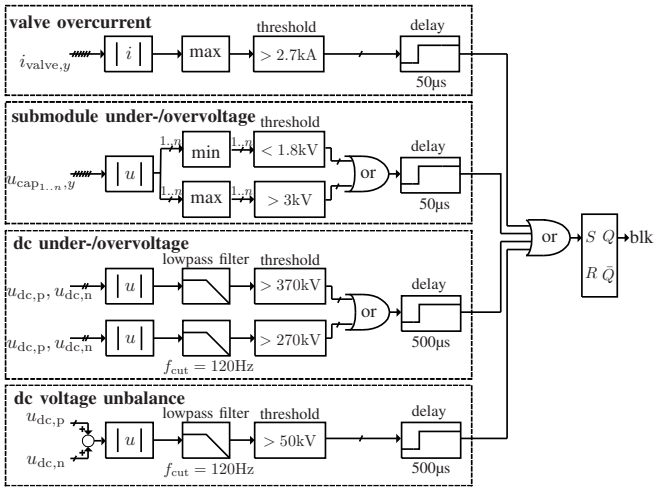

Fig. 14. Block diagram of considered protection scheme.

REFERENCES

[1] K. Sharifabadi, L. Harnefors, H.-P. Nee, S. Norrga, and R. Teodorescu, *Design, Control and Application of Modular Multilevel Converters for HVDC Transmission Systems*. Chichester, UK:John Wiley & Sons, Ltd,, Oct. 2016.

[2] G. Mazzanti and M. Marzinotto, *Extruded Cables For High-Voltage Direct-Current Transmission: Fundamentals of HVDC Cable Tranmission*. John Wiley & Sons, Inc., 2013, pp. 11–40.

[3] "Recommendations for testing DC extruded cable systems for power transmission at a rated voltage up to 500 kV," *CIGRE Tech. Rep. 496 (WG B1.31)*, 2012.

[4] IEC 62895:2017, "High voltage direct current (HVDC) power transmission - Cables with extruded insulation and their accessories for rated voltages up to 320 kV for land applications - Test methods and requirements," Tech. Rep., Nov. 2017.

[5] M. Saltzer et. al., "Surge and extended overvoltages testing of HVDC cable systems," *Int. Conf. on Insulated Power Cables (Jicable'17)*, no. Paper Jicable-HVDC17-S3.3, Dunkerque, France, Nov. 2017.

[6] M. Callavik, P. Lundberg, and O. Hansson, "NORDLINK Pioneering VSC-HVDC interconnector between Norway and Germany," in *a white Paper from ABB*, March 2015.

[7] Ø. Sagosen, A. Craig, R. Poole, R. Paradine, "Need, design and business case for building the North Sea Link," *CIGRE General Meeting*, Paris, France, Aug. 2018.

[8] V. Staudt et. al., "Control concept including validation strategy for an AC/DC hybrid link ("Ultranet")," in *2014 IEEE Energy Convers. Congr. and Expo. (ECCE)*, Sep. 2014, pp. 750–757.

[9] "Technical Requirements and Specifications of state-of-the-art HVDC Switching Equipment," *CIGRE Tech. Rep. 683 (WG A3/B4.34)*, 2017.

[10] F. B. Ajaei and R. Iravani, "Cable Surge Arrester Operation Due to Transient Overvoltages Under DC-Side Faults in the MMC-HVDC Link," *IEEE Trans. Power Del.*, vol. 31, no. 3, pp. 1213–1222, June 2016.

[11] S. Dennetière, H. Saad, A. Naud, P. Honda, "Transients on DC cables connected to VSC converters," *Int. Conf. on Insulated Power Cables (Jicable'15)*, Versailles, France, June 2015.

[12] M. Goertz et. al., "Overvoltage Characteristics in Symmetrical Monopole HB MMC-HVDC Configuration comprising Long Cable Systems," *Int. Conf. on Power System Transients (IPST'19)*, no. IPST19-039, Perpignan, France, June 2019.

[13] S. Mukherjee, M. Saltzer, Y.- J. Häfner, S. Nyberg, "Cable Overvoltages for MMC based VSC HVDC Systems: Interactions with Converters," *Int. Colloq. on H.V. Insulated Cables, CIGRE Study Committee B1*, New Delhi, India, Oct. 2017.

[14] H. Wang, J. Cao, Z. He, J. Yang, Z. Han, and G. Chen, "Research on Overvoltage for XLPE Cable in a Modular Multilevel Converter HVDC Transmission System," *IEEE Trans. Power Del.*, vol. 31, no. 2, pp. 683–692, April 2016.

[15] H. Saad, P. Rault, S. Dennetière, "Study on Transient overvoltages in the Converter Station of HVDC-MMC links," *Int. Conf. on Power System Transients (IPST'17)*, no. IPST17-185, Seoul, Republic of Korea, June 2017.

[16] M. Saltzer, M. Goertz, S. Wenig, W. Leterme et. al., "Overvoltage in Symmetric Monopolar HVDC Cable Systems - a Parameter Study Approach," in *CIGRE Symp. Aalborg - 2019, Paper no. 134*, June 2019.

[17] M. Greve, M. Koochack Zadeh, T. Rendel, A. Menze, "Behaviour of the HVDC links with MMC technology during DC cable faults," *CIGRE Winnipeg 2017 Colloq., Study Committees A3, B4 & D1*, Winnipeg, Canada, Sept. 2017.

[18] C. Freye, S. Wenig, M. Goertz, T. Leibfried, F. Jenau, "Transient Voltage Stresses in MMC-HVDC links - Impulse Analysis and Novel Proposals for Synthetic Laboratory Generation," *IET High Voltage*, vol. 3, no. 2, pp. 115–125, June 2018.

[19] T. Karmokar, M. Saltzer, S. Nyberg, S. Mukherjee, P. Lundberg, "Evaluation of 320 kV extruded DC cable system for temporary overvoltages by testing with very long impulse waveform," *CIGRE General Meeting*, Paris, France, Aug. 2018.

[20] M. Goertz et. al., "Analysis of Overvoltage Levels in the Rigid Bipolar MMC-HVDC Configuration," *15th IET Int. Conf. on AC and DC Power Trans. (ACDC 2018)*, Coventry, UK, Feb. 2019.

[21] S. Beckler, J. Reisbeck, F. Exl, F. Schell, "Approach for a comprehensive definition of the electrical interface between HVDC converter and cable," *Int. Conf. on Insulated Power Cables (Jicable'19)*, Versailles, France, June 2019.

[22] 50Hertz Transmission GmbH, Amprion GmbH, Tennet TSO GmbH, and TransentBw GmbH, "Grid Development Plan (GDP) 2030, version 2019, 2nd draft," *Technical Report, German Transmission System Operators*, Berlin, Germany, Apr. 2019.

[23] R. Li, J. E. Fletcher, and B. W. Williams, "Influence of third harmonic injection on modular multilevel converter -based high-voltage direct current transmission systems," *IET Gener., Transm. Dis.*, vol. 10, no. 11, pp. 2764–2770, 2016.

[24] C. Armschat, and M. Dommaschk, and V. Hussennether, and T. Westerweller, "Star-Point Reactor," *U.S. Patent US 2012/0120691 A1*, Jan. 12, 2012.

[25] F. Palone, M. Marzinotto, and L. Buono, "Temporary overvoltage mitigation in symmetrical monopole VSC-MMC HVDC links," in *2017 AEIT Int. Annual Conf.*, Sep. 2017, pp. 1–6.

[26] "MO Surge Arresters - Stresses and Test Procedures," *CIGRE Tech. Rep. 544 (WG A3.17)*, Aug., 2013.

[27] W. Leterme, P. Tielens, S. D. Boeck, and D. V. Hertem, "Overview of grounding and configuration options for meshed HVDC grids," *IEEE Trans. Power Del.*, vol. 29, no. 6, pp. 2467–2475, Dec. 2014.

[28] IEC TR 60071-4, "Insulation co-ordination- Part 4: Computational guide to insulation co-ordination and modelling of electrical networks, First edition," Tech. Rep., Apr. 2004.

[29] "Guide for the development of models for HVDC converters in a HVDC grid," *CIGRE Tech. Rep. 604 (WG B4.57)*, 2014.

[30] S. Wenig, M. Goertz, C. Hirsching, M. Suriyah, and T. Leibfried, "On Full-Bridge Bipolar MMC-HVDC Control and Protection for Transient Fault and Interaction Studies," *IEEE Trans. Power Del.*, vol. 33, no. 6, pp. 2864–2873, Dec. 2018.

[31] "Protection and Local Control of HVDC-Grids," *CIGRE Tech. Rep. 739 (WG B4/B5.59)*, Aug. 2018.

[32] A. Morched, B. Gustavsen and M. Tartibi, "A universal model for accurate calculation of electromagnetic transients on overhead lines and underground cables," *IEEE Trans. Power Del.*, vol. 14, no. 3, pp. 1032–1038, July 1999.

[33] G. Li, J. Liang, F. Ma, C. E. Ugalde-Loo, and H. Liang, "Analysis of single-phase-to-ground faults at the valve-side of hb-mmcs in hvdc systems," *IEEE Trans. Ind. Electron.*, vol. 66, no. 3, pp. 2444–2453, March 2019.

[34] G. Andersson, and M. Hytinnen, "Skagerrak The next generation," *CIGRE Symp. Lund - 2015*, Lund, Sweden, 2015.

[35] J. P. Kjaergaard et. al., "Bipolar operation of an HVDC VSC converter with an LCC converter," *CIGRE Colloq. on HVDC and Power Electron. Syst.*, San Francisco, USA, 2012.

Max Goertz was born in Ludwigshafen, Germany, in 1991. He received the M.Sc. degree in electrical engineering from the Karlsruhe Institute of Technology (KIT), Karlsruhe, Germany, in 2015, where he is currently working toward the Ph.D. degree in electrical engineering. His research interests include modeling of HVDC systems for EMT-type studies, control and protection of MMC-HVDC, as well as insulation co-ordination of HVDC equipment. Mr. Goertz is a member of VDE and CIGRE.

Simon Wenig (M'15) was born in Coburg, Germany, in 1985. He received the Dipl.-Ing. and Dr.-Ing. degree in electrical engineering from the Karlsruhe Institute of Technology, Karlsruhe, Germany, in 2013 and 2019, respectively. Since 2018, he joined the transmission system operator TransnetBW in Stuttgart, Germany, where he is currently involved in several ongoing embedded HVDC and STATCOM projects. His research interests include EMT-type studies and tools, MMC controls and dynamic performance as well as power-quality aspects of future grids. Mr. Wenig is a member of VDE and CIGRE and active in several international working groups.

Simon Beckler received his M.Sc. degree in Electrical Energy Engineering from the University of Stuttgart in 2014. After graduating he joined TransnetBW as HVDC engineer within the grid development department with a focus on grid integration of HVDC systems and dynamic and transient studies. Since 2019 he is working as HVDC system-technology engineer with a focus on system design aspects. Mr. Beckler is a member of VDE and CIGRE.

Carolin Hirsching was born in Bietigheim-Bissingen, Germany, in 1993. She received the M.Sc. degree in electrical engineering from the KIT, Karlsruhe, Germany in 2017, where she is currently persuing the Ph.D. degree in electrical engineering. Her research interests include MMC control strategies, acdc interactions and HVDC grids. Ms. Hirsching is a member of VDE and CIGRE.

Michael Suriyah (M'14) was born in Kuala Lumpur, Malaysia, in 1982. He received the diploma and M.Sc. degrees in electrical engineering from the University of Applied Sciences, Karlsruhe, Germany, in 2007 and 2008, respectively, and the Ph.D. degree in electrical engineering from the KIT, in 2013. Currently, he is the Head of the Department for Power Networks at the Institute of Electric Energy Systems and High-Voltage Technology. His research interests include aging diagnostics and onsite testing of power transformers, high-voltage testing methods, analysis of electric power networks as well as planning of future power systems. He is a member of VDE.

Thomas Leibfried (M'96) was born in Neckarsulm, Germany, in 1964. He received the Dipl.-Ing. and Dr.-Ing. degrees from the University of Stuttgart, Germany, in 1990 and 1996, respectively. From 1996 to 2002, he was with the Siemens AG, Nuremberg, Germany, working in the power transformer business in various technical and management positions. In 2002, he joined the University of Karlsruhe (now KIT), Karlsruhe, Germany, as Head of the Institute of Electric Energy Systems and High-Voltage Technology. He is a member of VDE and CIGRE.